Shock and Vibration 11 (2004) 173–186
IOS Press

Semi-active friction damping of large space truss structures

L. Gaul*, H. Albrecht and J. Wirnitzer
Institute A of Mechanics, University Stuttgart, Germany

The authors dedicate this paper to the memory of Professor Bruno Piombo.
We commemorate him as a vital contributor to our science. From the experience of sharing conferences and workshops with Bruno since many years, learning from his expertise and appreciating his advice, the first author mourns the loss of a good friend whose works and words will be kept in our minds and hearts.

Abstract. The present approach for vibration suppression of flexible structures is based on friction damping in semi-active joints. At optimal locations conventional rigid connections of a large truss structure are replaced by semi-active friction joints. Two different concepts for the control of the normal forces in the friction interfaces are implemented. In the first approach each semi-active joint has its own local feedback controller, whereas the second concept uses a global, clipped-optimal controller. Simulation results of a 10-bay truss structure show the potential of the proposed semi-active concept.

1. Introduction

Large space structures (LSS) are commonly designed as very flexible and lightweight truss structures of big size. Due to their small damping and the stringent positioning accuracy, many missions involving antennas or optical interferometers require vibration suppression. Numerous works have been published on active vibration suppression. Usually piezoelectric stacks are used as devices for actuators because of their light weight, high force and minimum power consumption. Although an active approach is very attractive, actively controlled systems may cause spillover instability. Passive approaches for damping enhancement involving visco-elastic materials or preloaded backlashes [20] may be desirable because of their simplicity and low cost. The present approach is based on friction damping in the joint connections of a truss structure [7]. Dry friction caused by slip in the interface of connected parts turns out to provide a significant amount of energy dissipation. The original truss nodes are modified such that relative slip between the truss member's end connector and the truss node is allowed.

However, passive approaches for vibration suppression are by far not as effective as active ones. Passive friction damping has several disadvantages. When the amplitude of vibration decreases below a certain level sticking occurs and energy is no longer dissipated. In addition, if the stiction force is quite high the connected parts can stick and thus static shape accuracy cannot be assured. To overcome these drawbacks, the friction force in the joint connection is controlled by varying the normal force in the contact interface using a piezoelectric stack [9]. Since a passive device is actively controlled, this approach is called semi-active. The resulting semi-active vibration suppression system is always stable, at least in the Lyapunov sense, because of the dissipative nature of friction. Another appeal of semi-active control is that performance levels of active control can be achieved with a fraction of input power. Furthermore, this concept can easily be employed without significantly increasing the structural weight.

The paper is structured as follows. It starts with the numerical model of the adaptive structure consisting of the truss structure which is considered as a linear subsystem and the nonlinear semi-active joints which exert state-dependent

*Corresponding author. E-mail: Gaul@mecha.uni-stuttgart.de.

ISSN 1070-9622/04/$17.00

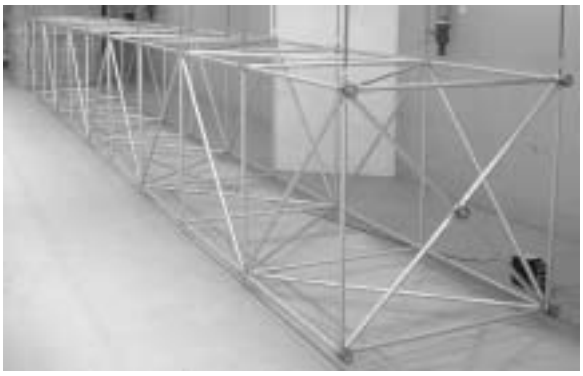

Fig. 1. Truss structure.

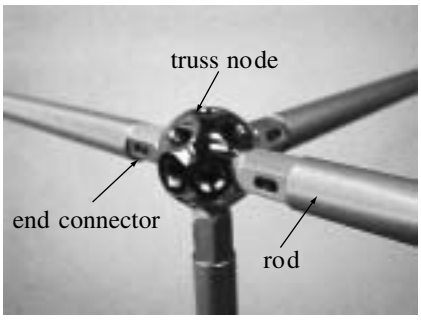

Fig. 2. Meroform components.

friction forces on the linear subsystem. The parameters of the nonlinear friction model must be identified from measurements conducted with an isolated joint. Based on the open-loop state space model of the linear subsystem, modal reduction is performed using controllability and observability gramians. To improve the fidelity of the reduced model for lower frequencies, the modal subspace is augmented with Krylov vectors.

At optimal locations conventional connections are replaced by semi-active friction joints and two different control concepts for the semi-active vibration suppression are introduced: local feedback control and clipped-optimal control. The simulation results for a 10-bay truss structure presented at the end reveal the potential of the presented semi-active approach.

2. Adaptive truss structure

The 10-bay truss structure depicted in Fig. 1 is made of Meroform-M12 construction system consisting of aluminium tubes connected by steel nodes. The Meroform components are shown in more detail in Fig. 2. Each tube has a 22 mm outer diameter and is fitted with a screw end connector. The horizontal and vertical distance between the center of the truss nodes is 1 m. In accordance with the Shuttle Radar Topography Mission (SRTM) [1] where a similar truss structure has been used as a cantilever to carry one of the two radar equipments, the mast is clamped at one end. At the free end a mass of 0.5 kg is attached to each of the five truss nodes.

For the implementation of the semi-active damping approach a modified joint connection has been designed, which allows relative motion between the end connector of a truss member and the truss node with the remaining members attached to it. The rigid Meroform nodes can be replaced by this adaptive joint. As shown in Fig. 3, two

[1] For details visit the websites http://www.jpl.nasa.gov/srtm/ and http://www.aec-able.com/corporate/srtm.htm.

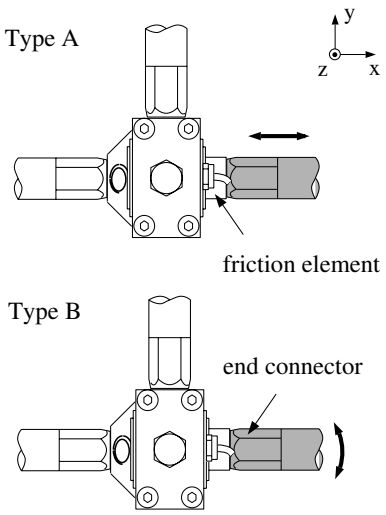

Fig. 3. Types of joints.

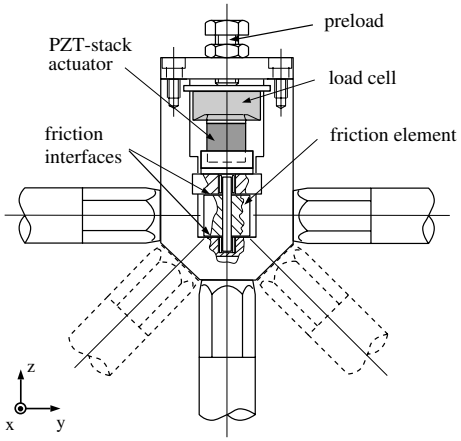

Fig. 4. Adaptive joint (type B).

types of joints are considered, each allowing relative motion in one particular degree-of-freedom. It is the relative displacement along the longitudinal axis of the connected rod, affecting the extensional stiffness of the connection (type A), and the relative rotation about an axis perpendicular to the longitudinal axis, affecting the bending stiffnes of the connection (type B).

A sketch of the rotational prototype (type B) is shown in Fig. 4. The semi-active joint employs the dissipative character of dry friction caused by interfacial slip in the contact area. [2] By applying voltage to the piezoelectrical stack actuator, the pressure in the contact area can be altered. The normal force is approximately proportional to the applied voltage. The preload of the stack can be adjusted by a screw.

[2] L. Gaul: German Patent “Smart Joint”, Number 19702518 C2 (1997).

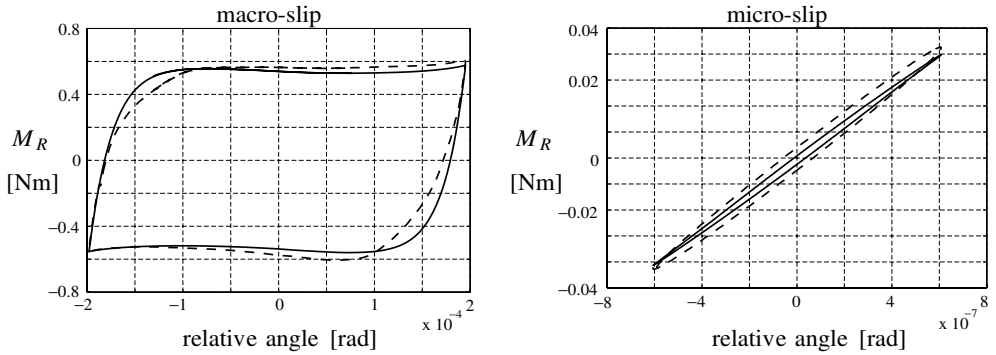

Fig. 5. Hysteresis loops for type B: simulation (—), experiment (– – –).

3. Numerical model

3.1. Model of the friction joint

For the modeling of the nonlinear behaviour in the friction joints the so called LuGre-model [3] has been proposed [9] which is capable of simulating relevant friction phenomena [1], such as presliding displacement, stick-slip and the Stribeck effect. It describes the friction interface as a contact between bristles. The internal state variable φ representing the average deflection of the bristles is governed by the first order differential equation

$$\begin{aligned} \dot{\varphi} &= f(v,\varphi) = v - \sigma_0 g(v)\,\varphi \qquad \text{with} \\ g(v) &= \frac{|\,v\,|}{F_c + F_d e^{-(v/v_s)^2}} \end{aligned} \tag{1}$$

where v is the relative sliding velocity in the contact. The friction force transmitted in the joint

$$F_R = F_N \underbrace{(\sigma_0\,\varphi + \sigma_1\,\dot{\varphi} + \sigma_2\,v)}_{=:\mu\,(v,\,\varphi)} \tag{2}$$

depends on the normal force F_N and the dynamic friction coefficient $\mu(v,\varphi)$. In case of a rotational joint (type B), a radius r is introduced in equation (2) to obtain a friction moment, i.e., $M_R = r\,F_R$, where v represents the relative angular velocity. In the following, for both types the generalised force u_R and the generalised sliding velocity v will be used. The model parameters $\sigma_{0_k}, \sigma_{1_k}, \sigma_{2_k}, F_{c_k}, F_{d_k}$ and v_{s_k} are all positive and have dimensions consistent with the dimension of v.

3.2. Parameter identification

In order to identify the parameters of the LuGre-model, the transfer behaviour of an isolated friction joint is measured. The joint is supported on a foundation and the friction element (see Fig. 4) is harmonically excited by a shaker. The sliding velocity and the excitation force are recorded for different normal forces and different excitation amplitudes and frequencies. Based on the known inertia the transmitted friction force can be calculated from the measured excitation force.

The model parameters are determined from the comparison between the simulated response and the measurements. This is done by solving the optimization problem

$$\min_{\boldsymbol{p}} \mathcal{J}(\boldsymbol{p}) = \frac{1}{2}\sum_{k=0}^{K} \left[u_R(t_k) - \hat{u}_R(v(t_k), F_N, \boldsymbol{p})\right]^2 \tag{3}$$

with the vector $\boldsymbol{p}$ containing the parameters to be identified, the measured friction force $u_R(t_k)$ and the simulated friction force $\hat{u}_R(v(t_k), F_N, \boldsymbol{p})$, which is obtained from Eq. (2) and integration of Eq. (1). For calculation of $\hat{u}_R$ the measured sliding velocity $v(t_k)$ and normal force F_N which is kept constant during the recording period are used.

Table 1
Identified friction parameters

Typ	σ_0	σ_1	σ_2	F_c	F_d	v_s	r
A	$1.42 \cdot 10^5\,1/\mathrm{m}$	$0.02\,\mathrm{s/m}$	$0.01\,\mathrm{s/m}$	0.61	0.14	$0.01\,\mathrm{m/s}$	–
B	$6.5 \cdot 10^4\,1/\mathrm{rad}$	$0.02\,\mathrm{s/rad}$	$0.01\,\mathrm{s/rad}$	0.49	0.08	$0.02\,\mathrm{rad/s}$	$0.011\,\mathrm{m}$

From the results of a fuzzy sensitivity analysis [13] it is known, that the individual parameters are responsible for different behaviour characteristics. Micro-slip behaviour is mostly affected by the parameters $\boldsymbol{p}_1 = [\sigma_0\ \sigma_1]$. During macro-slip, where sliding in the entire contact area occurs, especially the parameters $\boldsymbol{p}_2 = [F_c\ F_d\ v_s\ \sigma_2]$ are of importance. Macro-slip and micro-slip behaviour can be generated by choosing an appropriate combination of excitation amplitude and normal force which has an influence on the break-away force.

To efficiently solve the optimization problem in Eq. (3), the identification is carried out in two steps. First, the parameters $\boldsymbol{p}_1$ are identified from responses measured during micro-slip regime. The remaining parameters $\boldsymbol{p}_2$ are obtained from measurements where the joint is operated in stick-slip behaviour. For both optimizations, data from several measurements with different excitations and normal forces are used. Because of the nonlinear objective function Eq. (3) a gradient-based optimization algorithm will only give local minima. Therefore, it is important to start the optimization with reasonable initial values for $\boldsymbol{p}_1$ and $\boldsymbol{p}_2$.

The identified parameters are listed in Table 1 for both types of the joint. The present joint design turned out to have quite small parameters σ_1 und σ_2 which have almost no influence on the dynamical behaviour. A fact that is confirmed by the results of the fuzzy sensitivity analysis [13]. Therefore, it is hard to identify their actual values. As an example, one of the measured hysteresis loops for type B is compared to the predicted loop in Fig. 5.

3.3. FE-model of the truss structure

The FE discretization of the truss connections is depicted in Fig. 6. All tubes and end connectors are discretized by cubic Euler-Bernoulli beams with two nodes, each having six degrees of freedom. The Meroform nodes are considered as perfectly rigid and the rigid portions are modelled by geometric constraints $\boldsymbol{u}_m = \boldsymbol{S}_{nm}\boldsymbol{u}_n$ between the tied dofs $\boldsymbol{u}_m$ and the independent dofs $\boldsymbol{u}_n$. The mass and inertia of the Meroform connections are lumped at the centers of each truss node. The kinematics of the friction joints are described by constraint matrices, as well, which couple the degrees of freedom of the corresponding nodes according to the type of joint. By assembling all constraint matrices $\boldsymbol{S}_{nm}$ into matrix $\boldsymbol{S}$, all dependent degrees of freedom of the original finite element model with mass matrix $\bar{\boldsymbol{M}}$, damping matrix $\bar{\boldsymbol{D}}$, stiffness matrix $\bar{\boldsymbol{K}}$ and the displacement vector $\bar{\boldsymbol{z}}$ can be eliminated as follows

$$\begin{aligned} &\boldsymbol{S}^T\bar{\boldsymbol{M}}\boldsymbol{S}\ddot{\bar{\boldsymbol{z}}} + \boldsymbol{S}^T\bar{\boldsymbol{D}}\boldsymbol{S}\dot{\bar{\boldsymbol{z}}} + \boldsymbol{S}^T\bar{\boldsymbol{K}}\boldsymbol{S}\bar{\boldsymbol{z}} \\ &\quad = \boldsymbol{S}^T\bar{\boldsymbol{E}}\,\boldsymbol{u}_R(\boldsymbol{v},\boldsymbol{\varphi}) + \boldsymbol{S}^T\bar{\boldsymbol{F}}\boldsymbol{w}\ . \end{aligned} \tag{4}$$

The resulting system of differential equations is given by

$$\boldsymbol{M}\ddot{\boldsymbol{z}} + \boldsymbol{D}\dot{\boldsymbol{z}} + \boldsymbol{K}\boldsymbol{z} = \boldsymbol{E}\,\boldsymbol{u}_R(\boldsymbol{v},\boldsymbol{\varphi}) + \boldsymbol{F}\boldsymbol{w} \tag{5}$$

with the vector $\boldsymbol{z}$ containing only the independent generalised displacements z_j $(j = 1,\ldots,N)$. The friction forces $\boldsymbol{u}_R(\boldsymbol{v},\varphi)$ acting in the friction joints depend on the sliding velocities $\boldsymbol{v} = \boldsymbol{E}^T\dot{\boldsymbol{z}}$ and the bristle deflections $\boldsymbol{\varphi}$. Vector $\boldsymbol{w}$ represents disturbances.

Using the modal trasformation

$$\boldsymbol{z}(t) = \Phi\boldsymbol{\eta}(t) \tag{6}$$

with the modal matrix $\Phi = [\boldsymbol{\phi}_1,\ldots,\boldsymbol{\phi}_n]$ (including $n < N$ 'significant' eigenmodes $\boldsymbol{\phi}_i$) obtained from the undamped eigenvalue problem

$$\boldsymbol{K}\boldsymbol{\phi}_i = \omega_i^2\boldsymbol{M}\boldsymbol{\phi}_i\ , \qquad i = 1,\ldots,n \tag{7}$$

and assuming modal damping, Eq. (5) can be transformed to a set of differential equations

$$\ddot{\boldsymbol{\eta}} + \Xi\dot{\boldsymbol{\eta}} + \Omega\boldsymbol{\eta} = \Phi^T\boldsymbol{E}\,\boldsymbol{u}_R(\boldsymbol{v},\boldsymbol{\varphi}) + \Phi^T\boldsymbol{F}\boldsymbol{w} \tag{8}$$

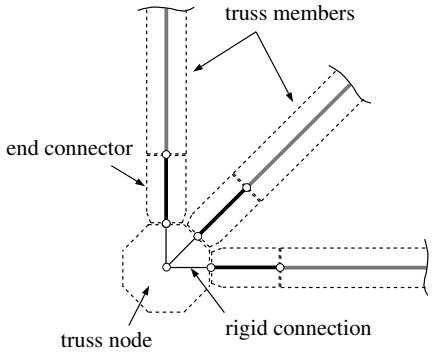

Fig. 6. FE discretization.

No	EMA	FEM	error [%]	MAC
1	4.49	4.495	0.18	0.79
2	4.60	4.595	0.19	0.88
3	20.65	20.60	0.24	0.97
4	22.07	22.25	0.82	0.95
5	23.61	23.76	0.64	0.93
7	24.72	25.08	1.46	0.93
8	43.47	43.73	0.60	0.95
12	46.83	46.90	0.15	0.98
17	49.45	49.52	0.14	0.72

Fig. 7. Eigenfrequencies in [Hz].

with the matrices $\Omega = \mathrm{diag}\,(\omega_i^2)$, $\Xi = \mathrm{diag}\,(2\xi_i\,\omega_i)$ and the vector $\boldsymbol{\eta}$ of modal coordinates η_i. The eigenfrequency and the modal damping coefficient of the i-th mode is denoted by ω_i and ξ_i, respectively.

The sliding velocities $\boldsymbol{v}$ and the measured states $\boldsymbol{y}$, which in chapters 4.3 and 6 will be the deflections of the tip of the mast, are given by

$$\boldsymbol{v} = \boldsymbol{E}^T \Phi\, \dot{\boldsymbol{\eta}} \tag{9}$$

$$\boldsymbol{y} = \boldsymbol{V}\Phi\boldsymbol{\eta} + \boldsymbol{W}\Phi\dot{\boldsymbol{\eta}}\ . \tag{10}$$

It should be pointed out that the transformation matrix in Eq. (6) is composed of eigenvectors of the underlying linear undamped system. That means, the nonlinear state-dependent term in the excitation vector $\boldsymbol{u}_R$ is neglected and a truss structure with frictionless joint connections is considered, i.e. $F_{N_j} = 0$. That way, the structure of the linear subsystem can fully be exployed for the upcoming model reduction. Such an approach is often used for systems with local nonlinearities [16].

Since not all the parameters of the FE model are known a priori, they have to be identified by means of Modal Updating [6] using eigenfrequencies and mode shapes obtained from an Experimental Modal Analysis (EMA) which has been performed on the structure. The unknown parameters particularly are the axial, bending and torsional stiffness of the end connectors. Furthermore, the material properties of the aluminum members are not exactly known. Dimensions and masses of the components however are considered as given.

The eigenfrequencies calculated with the updated FE model are compared to the measured values in Table 7. The corresponding MAC values [6] of the mode shapes are listed as well. Note that only those modes are listed whose mode shapes could clearly be identified by the EMA. The extracted modal damping ratios $0.05\% \leqslant \xi_i \leqslant 0.5\%$ confirm that the present strutcture indeed is a weakly damped system. For the upcoming simulations $\xi_i = 0.1\%$ will be used for all modes $i = 1, \ldots, n$.

3.4. Model of the adaptive structure

By defining the state vector of the linear subsystem as

$$\boldsymbol{x} = \left[\boldsymbol{x}_1^T, \ldots, \boldsymbol{x}_n^T\right]^T \text{ with } \boldsymbol{x}_i = \begin{bmatrix} \dot{\eta}_i \\ \omega_i \eta_i \end{bmatrix} \tag{11}$$

where the state $\boldsymbol{x}_i$ represents the i-th mode, the state space form of the friction damped truss structure is given by

$$\begin{bmatrix} \dot{\boldsymbol{x}} \\ \dot{\boldsymbol{\varphi}} \end{bmatrix} = \begin{bmatrix} \boldsymbol{A}\boldsymbol{x} \\ \boldsymbol{f}(\boldsymbol{v}, \boldsymbol{\varphi}) \end{bmatrix} + \begin{bmatrix} \boldsymbol{B} \\ 0 \end{bmatrix} \boldsymbol{u}_R(\boldsymbol{v}, \boldsymbol{\varphi}) + \begin{bmatrix} \boldsymbol{H} \\ 0 \end{bmatrix} \boldsymbol{w} \; . \tag{12}$$

The system matrix $\boldsymbol{A}$ as well as the matrices $\boldsymbol{B}$ and $\boldsymbol{H}$ can easily be deduced from Eq. (5) by taking the definition of the state vector $\boldsymbol{x}$ into account. The internal state variables φ_j $(j = 1, \ldots, l)$ of the l semi-active friction joints are arranged in $\boldsymbol{\varphi}$, the corresponding differential Eq. (1) in $\boldsymbol{f}(\boldsymbol{v}, \boldsymbol{\varphi})$. The sliding velocities are given by $\boldsymbol{v} = \boldsymbol{B}^T \boldsymbol{x}$. The actuator forces $\boldsymbol{u}_R$ are defined by Eq. (2) as $\boldsymbol{u}_{R_j} = F_{N_j}\, \mu_j(v_j, \varphi_j)$ where the normal forces F_{N_j} represent the controller output.

4. Model reduction

Because of the high order of the system Eq. (12), a model reduction is required to obtain a low order model for the control design. This is done by significantly reducing the order of the linear subsystem and keeping the nonlinear part unchanged. Thus, the linear subsystem

$$\begin{bmatrix} \dot{\boldsymbol{x}}_d \\ \dot{\boldsymbol{x}}_{nd} \end{bmatrix} = \begin{bmatrix} \boldsymbol{A}_d & 0 \\ 0 & \boldsymbol{A}_{nd} \end{bmatrix} \begin{bmatrix} \boldsymbol{x}_d \\ \boldsymbol{x}_{nd} \end{bmatrix} + \begin{bmatrix} \boldsymbol{B}_d \\ \boldsymbol{B}_{nd} \end{bmatrix} \boldsymbol{u} + \begin{bmatrix} \boldsymbol{H}_d \\ \boldsymbol{H}_{nd} \end{bmatrix} \boldsymbol{w} \tag{13}$$

$$\boldsymbol{v} = \begin{bmatrix} \boldsymbol{B}_d^T \; \boldsymbol{B}_{nd}^T \end{bmatrix} \begin{bmatrix} \boldsymbol{x}_d \\ \boldsymbol{x}_{nd} \end{bmatrix} \tag{14}$$

$$\boldsymbol{y} = \begin{bmatrix} \boldsymbol{C}_d \; \boldsymbol{C}_{nd} \end{bmatrix} \begin{bmatrix} \boldsymbol{x}_d \\ \boldsymbol{x}_{nd} \end{bmatrix} \tag{15}$$

is considered in the following. It is partitioned into dominant states $\boldsymbol{x}_d$ which will be kept in the reduced model, and states $\boldsymbol{x}_{nd}$ which will be removed. In the following considerations, the nonlinear friction forces $\boldsymbol{u}_R$ are neglected and the vector $\boldsymbol{u}$ represents external (state-independent) actuator forces.

4.1. Balanced reduction

The determination of dominant modes $\boldsymbol{x}_{d_i}$ is based on balanced reduction using controllability and observability gramians corresponding to the different inputs ($\boldsymbol{u}$, $\boldsymbol{w}$) and outputs ($\boldsymbol{v}$, $\boldsymbol{y}$) of the system. For an asymptotically stable system, the controllability gramian $\boldsymbol{W}^c$ and observability gramian $\boldsymbol{W}^o$ are symmetric and positive definite matrices which can be computed from the steady-state Lyapunov equations [19]

$$\begin{aligned} &\boldsymbol{A}\boldsymbol{W}^c + \boldsymbol{W}^c\boldsymbol{A}^T + \boldsymbol{B}\boldsymbol{B}^T = 0 \text{ and} \\ &\boldsymbol{A}^T\boldsymbol{W}^o + \boldsymbol{W}^o\boldsymbol{A} + \boldsymbol{C}^T\boldsymbol{C} = 0 \; . \end{aligned} \tag{16}$$

Due to the particular form of the state space model with modal coordinates, Eq. (16) can be solved in closed form [11]. For structures with small damping and well separated eigenfrequencies [3] the gramians tend to diagonal matrices

[3] Even for truss structures with their quite high modal density, this approximation is valid as long as the damping ratios are small, i.e., $\xi_i \ll 1$ [11,12].

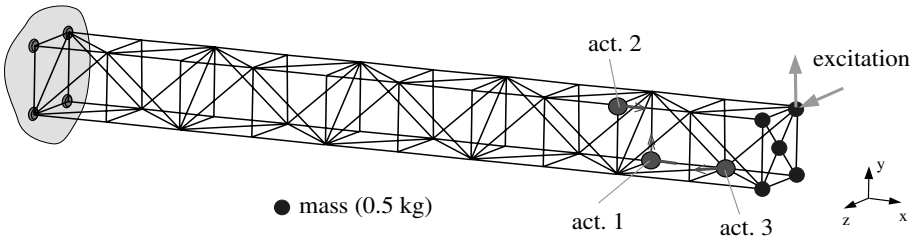

Fig. 8. Example: Structure with semi-active joints.

$$\boldsymbol{W}^{c(o)} = \mathrm{diag}\begin{pmatrix} w_i^{c(o)} & 0 \\ 0 & w_i^{c(o)} \end{pmatrix} \text{ with}$$
$$w_i^c = u_i \frac{\boldsymbol{e}_i \boldsymbol{e}_i^T}{4\xi_i\omega_i}\ ,\ w_i^o = \frac{\omega_i^2 \boldsymbol{w}_i^T \boldsymbol{w}_i + \boldsymbol{v}_i^T \boldsymbol{v}_i}{4\xi_i\omega_i^3} \tag{17}$$

where $i = 1, \ldots, n$. The vector $\boldsymbol{e}_i$ is the i-th row of $\Phi^T \boldsymbol{E}$, vectors $\boldsymbol{v}_i$ and $\boldsymbol{w}_i$ correspond to the i-th column of $\boldsymbol{V}\Phi$ and $\boldsymbol{W}\Phi$, respectively. The i-th diagonal element w_i^c (w_i^o) is a quantitative measure for the controllability (observability) of the i-th state $\boldsymbol{x}_i = [\dot{\eta}_i, \omega_i\eta_i]^T$ which represents the i-th mode.

To idenfity modes which are relevant for the transfer behaviour of the input/output path from $\boldsymbol{u}_R$ to $\boldsymbol{v}$, one has to check the corresponding Hankel singular values [12]

$$\gamma_{uv_i} = \sqrt{w_{u_i}^c\, w_{v_i}^o} = \frac{\boldsymbol{e}_i \boldsymbol{e}_i^T}{4\xi_i\omega_i} \tag{18}$$

defined by means of the eigenvalues of the controllability and observability gramians for the input $\boldsymbol{u}$ and output $\boldsymbol{v}$, i.e., $w_{u_i}^c$ and $w_{v_i}^o$ respectively. Modes with large Hankel singular values γ_{uv_i} should be included into the reduced model in order to guarantee a good approximation of the original system. Those modes will mainly be excited by the friction forces. And they will contribute to the sliding velocities $\boldsymbol{v}$ occuring in the friction joints, as well.

In addition, all modes which have an impact on the system measurements $\boldsymbol{y}$ need to be added to the reduced model. They are selected according to the eigenvalues $w_{y_i}^o$ of the observability gramian corresponding to the output $\boldsymbol{y}$. When the disturbance input matrix $\boldsymbol{H}$ is known, it can be taken into account as well.

4.2. Krylov vectors

After the dominant states are choosen, the reduced model of the linear subsystem is given by

$$\dot{\boldsymbol{x}}_d = \boldsymbol{A}_d\boldsymbol{x}_d + \boldsymbol{B}_d\tilde{\boldsymbol{u}}_R(\tilde{\boldsymbol{v}}, \boldsymbol{\varphi}) + \boldsymbol{H}_d\boldsymbol{w} \tag{19}$$
$$\tilde{\boldsymbol{v}} = \boldsymbol{B}_d^T\boldsymbol{x}_d = \boldsymbol{E}^T\Phi_d\dot{\boldsymbol{\eta}}_d \tag{20}$$
$$\tilde{\boldsymbol{y}} = \boldsymbol{C}_d\boldsymbol{x}_d = \boldsymbol{V}\Phi_d\boldsymbol{\eta}_d + \boldsymbol{W}\Phi_d\dot{\boldsymbol{\eta}}_d\ . \tag{21}$$

Now, focus on the input/output path from $\boldsymbol{u}_R$ to $\boldsymbol{v}$ which is the most critical since the prediction of the local nonlinearities is affected by the approximation quality of this path. As a result of neglecting the part $\boldsymbol{B}_{nd}^T\boldsymbol{x}_{nd}$ in Eq. (20), the approximated sliding velocity $\tilde{\boldsymbol{v}}$ is erroneous. This has a negative effect on the prediction of the resulting friction forces $\tilde{\boldsymbol{u}}_R(\tilde{\boldsymbol{v}}, \boldsymbol{\varphi})$. The approximation error would amplify when simulating the closed-loop system. Therefore, it is important to somehow compensate for the deleted modes. For this purpose the transfer matrix $\boldsymbol{G}^{uv}(s)$ from $\boldsymbol{u}$ to $\boldsymbol{v}$

$$\boldsymbol{G}^{uv}(s) = \boldsymbol{B}^T(s\boldsymbol{I} - \boldsymbol{A})^{-1}\boldsymbol{B} = \underbrace{\boldsymbol{B}_d^T(s\boldsymbol{I}_d - \boldsymbol{A}_d)^{-1}\boldsymbol{B}_d}_{=:\boldsymbol{G}_d^{uv}(s)} + \boldsymbol{G}_{nd}^{uv}(s) \tag{22}$$

is considered. The term $\boldsymbol{G}_{nd}^{uv}$ corresponds to the neglected $n_{nd} = N - n_d$ modes. The coefficients $\mathcal{H}_k = \mathcal{H}_{d_k} + \mathcal{H}_{nd_k}$ of a Taylor series around $s_0 = 0$

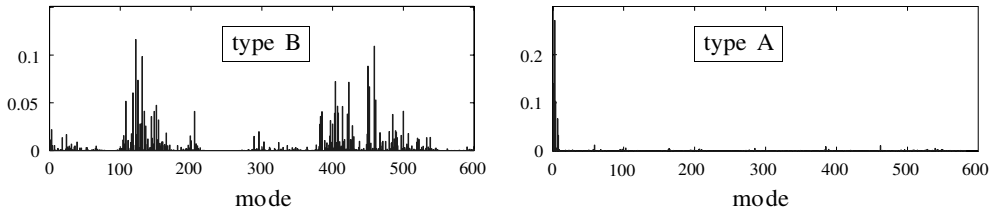

Fig. 9. Eigenvalues $w_{u_i}^c$.

$$\boldsymbol{G}^{uv}(s) = \sum_{k=0}^{N_k} \underbrace{(-1)^{k+1}\boldsymbol{B}^T\boldsymbol{A}^{-k-1}\boldsymbol{B}}_{=:\mathcal{H}_k(0)} s^k = \sum_{k=0}^{N_k} \Big(\mathcal{H}_{d_k}(0) + \mathcal{H}_{nd_k}(0)\Big) s^k \tag{23}$$

are the so called 'low order moments' which are used in 'moment matching methods' for model reduction purposes [4]. Considering the j-th friction joint, the first ($k = 0$) correction term $\mathcal{H}_{nd_0}$ for the second order system in Eq. (5) is given by

$$\mathcal{H}_{nd_0} = \mathcal{H}_0 - \mathcal{H}_{d_0} = \boldsymbol{e}_j^T \left(\boldsymbol{K}^{-1}\boldsymbol{e}_j - \Phi_d\Omega_d^{-1}\Phi_d^T\boldsymbol{e}_j\right) = \boldsymbol{e}_j^T \left(\boldsymbol{I} - \Phi_d\Phi_d^T\boldsymbol{M}\right)\boldsymbol{K}^{-1}\boldsymbol{e}_j \tag{24}$$

when no damping is assumed[4], $\boldsymbol{e}_j$ being the j-th column of the matrix $\boldsymbol{E}$. $\mathcal{H}_{nd_0}$ represents the difference between the static deformation $\boldsymbol{K}^{-1}\boldsymbol{e}_j$ caused by an unit load acting in the j-th joint and the deformation $\Phi_d\Omega_d^{-1}\Phi_d^T\boldsymbol{e}_j$ which results from the mode superposition of the modes Φ_d. By taking further coefficients $\mathcal{H}_{nd_k}$ into account, the following recursive formula (Arnoldi process)

$$\boldsymbol{\psi}_k^* = \boldsymbol{K}^{-1}\boldsymbol{M}\boldsymbol{\psi}_{k-1}\boldsymbol{\psi}_k^{**} = \big(\boldsymbol{I} - \Sigma_{k-1}\Sigma_{k-1}^T\boldsymbol{M}\big)\boldsymbol{\psi}_k^*\boldsymbol{\psi}_k = \boldsymbol{\psi}_k^{**}\left(\boldsymbol{\psi}_k^{**^T}\boldsymbol{M}\boldsymbol{\psi}_k^{**}\right)^{-\frac{1}{2}} \tag{25}$$

for the calculation of so called Krylov vectors [2] can be derived. The starting vector is choosen as $\boldsymbol{\psi}_0 = \boldsymbol{K}^{-1}\boldsymbol{e}_j$. The matrix $\Sigma_k = [\Phi_d\ \boldsymbol{\psi}_1\ \ldots\ \boldsymbol{\psi}_{k-1}]$ contains not only the eigenvectors of Φ_d but the new generated vectors $\boldsymbol{\psi}_{k-1}$ ($k > 1$) as well. Thus, the bracket term in Eqs (26) and (27) constitute an orthonormalization with respect to the mass matrix. By generating K vectors for each friction joint j, a total number of $l \cdot K$ Krylov vectors is obtained. Since the columns of $\Psi = [\boldsymbol{\psi}_1\ \ldots\ \boldsymbol{\psi}_{lK}]$ are not orthogonal with respect to the stiffness matrix, a singular value decomposition (SVD)

$$\Psi^T\boldsymbol{K}\Psi = \boldsymbol{T}\hat{\Omega}\boldsymbol{T} \text{ where } \hat{\Omega} = \operatorname{diag}\left(\hat{\omega}_m^2\right), m = 1, \ldots, lK \tag{26}$$

is used to yield vectors $\hat{\Psi} = \Psi\boldsymbol{T}$ which also diagonalize the stiffness matrix.

When the transformation

$$\boldsymbol{z}(t) = [\Phi_d\ \hat{\Psi}]\begin{bmatrix}\boldsymbol{\eta}_d\\ \hat{\boldsymbol{\eta}}\end{bmatrix} \text{ with} \hat{\Psi} = [\hat{\boldsymbol{\psi}}_1\ \ldots\ \hat{\boldsymbol{\psi}}_{lK}] \text{ and } \hat{\boldsymbol{\eta}} = [\hat{\eta}_1\ \ldots\ \hat{\eta}_{lK}]^T\ , \tag{27}$$

is applied instead of Eq. (16), the reduced model Eq. (19) is extended by the additional rows

$$\ddot{\hat{\eta}}_m + 2\hat{\xi}_m\,\hat{\omega}_m\,\dot{\hat{\eta}}_m + \hat{\omega}_m^2\,\hat{\eta}_m = \hat{\boldsymbol{\psi}}_m^T\boldsymbol{E}\tilde{\boldsymbol{u}}_R^*(\tilde{\boldsymbol{v}}^*, \boldsymbol{\varphi}) + \hat{\boldsymbol{\psi}}_m^T\boldsymbol{F}\boldsymbol{w}\ , \qquad m = 1, \ldots, lK \tag{28}$$

And the expression for the approximated sliding velocity is

$$\tilde{\boldsymbol{v}}^* = \boldsymbol{E}^T\Phi_d\dot{\boldsymbol{\eta}}_d + \boldsymbol{E}\hat{\Psi}\dot{\hat{\boldsymbol{\eta}}}\ . \tag{29}$$

The last expression in Eq. (31) can be seen as a correction term which reduces the approximation error for low frequencies by compensating for the neglected modes of the original system. This also improves the approximated friction forces $\boldsymbol{u}_R^*$.

[4]Similar expressions can be given for damped second order systems [4]

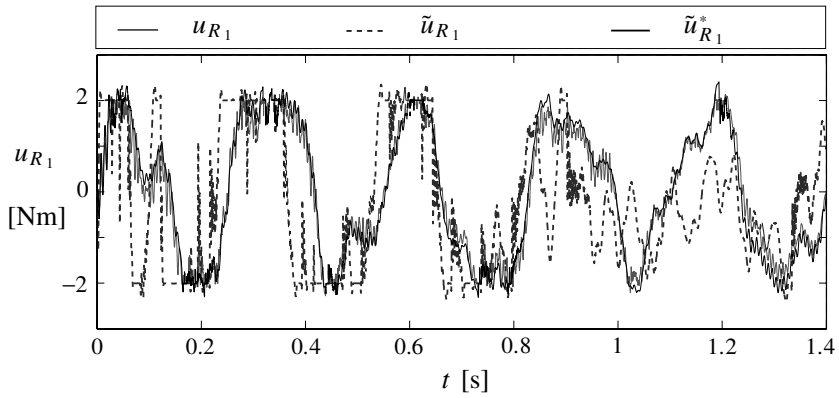

Fig. 10. Approximation of the friction moment u_{R_1}.

4.3. Example

As an example, the proposed reduction method is now applied to the 10-bay truss structure illustrated in Fig. 8. The displacements in y- and z-direction at the sensor location are used as measurements $\boldsymbol{y}$. The disturbance $\boldsymbol{w}$ is a triangular pulse in y- and z-direction which acts as a force at the mast tip as shown in Fig. 8.

For the present example a configuration with three friction joints (two of type A and one of type B) is used. Figure 9 shows the first $n = 600$ eigenvalues w_i^c of the controllability gramian for the rotational joint (type B) and for one of the translational joints (type A). As can be seen, the frictional forces caused by type A mainly affect the lowest modes whereas those caused by type B also excites higher modes. Therefore, only the friction joint of type B (actuator 1) will be considered as 'active', in order to point out the effect of the correction term $\boldsymbol{E}\,\hat{\Psi}\dot{\hat{\boldsymbol{\eta}}}$ in Eq. (31) on the approximation of the sliding angular velocity $\tilde{v}_1$ and the friction moment $\tilde{u}_{R_1}$. In the other two joints of type A no friction forces are transmitted and they are regarded as frictionless joint connections with zero normal force ($F_{N_{2,3}} = 0$). The reason for using those 'inactive' joints anyway is the resulting local stiffness reduction which is necessary for a significant effect of the rotational joint to occur.

Using the procedure from Section 4.1 $n_d = 60$ dominant modes are selected from the first $n = 100$. All higher modes are not included in the reduced model despite their large eigenvalues [5]. For a constant normal force $F_{N_1} = 400\,\mathrm{N}$, the friction moment $\tilde{u}_{R_1}$ of the reduced system given by Eq. (19) is plotted in Fig. 10 together with the friction moment obtained from the original system Eq. (5). It is obvious that the approximation of the actual friction moment is quite bad.

However, augmenting the modal subspace spanned by the eigenvectors $\boldsymbol{\phi}_{d_i}$ with just two Krylov vectors $\hat{\boldsymbol{\psi}}_{1,2}$ ($l = 1\,,\ k = 1, 2$) improves the low frequency approximation remarkably, as can be seen from the time signal of $\tilde{u}^*_{R_1}$ in Fig. 10.

5. Semi-active control

In the following, two different control approaches are proposed. In the first approach each semi-active friction joint has its own local feedback controller. The second concept uses one global clipped-optimal controller.

5.1. Local feedback control

Several semi-active control laws for friction dampers have been derived [18]. A bang-bang controller can be designed by inspection of the time derivative of the Lyapunov function representing the system energy. For the

[5] The numbers n and n_d are determined quite arbitrarily just to point out the effect of the correction term. An optimization of the ratio of n_d to the number of Krylov vectors is not considered in this paper.

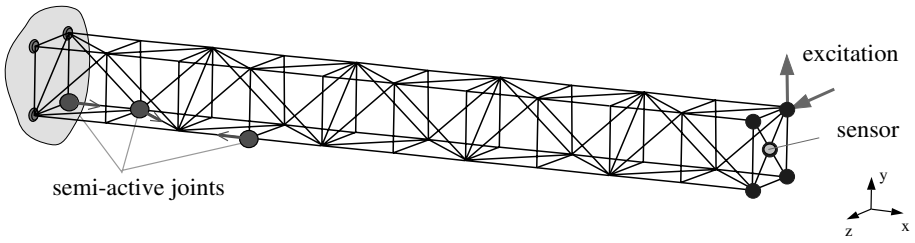

Fig. 11. Structure with three semi-active joints at optimal positions.

LuGre friction model defined by Eqs (2) and (1), one arrives at the feedback law

$$F_{N_j} = \begin{cases} F_{N_j}^{\max} & , \mu_j\, v_j \geqslant \varepsilon_j \\ F_{N_j}^{\min} + (F_{N_j}^{\max}/\varepsilon_j)\, \mu_j\, v_j & , 0 < \mu_j\, v_j < \varepsilon_j \\ F_{N_j}^{\min} & , \mu_j\, v_j \leqslant 0 \end{cases} \tag{30}$$

which maximizes the energy dissipation in the adaptive joint by avoiding sticking. A boundary layer ε_j has been introduced to avoid chattering (quasi-sticking) which degrates the energy dissipation. The dynamic friction coefficient μ_j is obtained from the relation

$$\mu_j(t) = \frac{u_{R_j}(t - \Delta t)}{F_{N_j}(t - \Delta t)} \tag{31}$$

where $1/\Delta t$ is the sampling rate of the controller.

It is assumed that besides the sliding velocities $\boldsymbol{v}$ the friction forces $\boldsymbol{u}_R$ can be measured, as well. Otherwise they have to be estimated using a simple integrator model as proposed by [14] or the dynamic friction coefficients μ_j have to be observed using an extended Kalman filter [8,10].

For an efficient vibration suppression, the control parameters ε_j of the SISO-controller are optimized [21] with respect to the system energy given by

$$E(t_e) = \int_0^{t_e} \left(\boldsymbol{x}^T \boldsymbol{x}\right)\, \mathrm{d}t\ . \tag{32}$$

5.2. Clipped-optimal control

For the second approach a so called clipped-optimal controller is used [5]. First, a LQG controller [17] is designed assuming an active control system and neglecting the actuator dynamics. The optimal actuator forces

$$\boldsymbol{u}_d = -\boldsymbol{K}\, \hat{\boldsymbol{x}} \tag{33}$$

are defined by the gain matrix $\boldsymbol{K}$, which is obtained as a solution of the algebraic Riccati equation [17] and the state vector $\hat{\boldsymbol{x}}$ is estimated by means of a Kalman filter [15].

The actuator forces $\boldsymbol{u}_d$ cannot directly be applied to the structure, they have to be generated by the semi-active friction dampers. This is achieved by controlling the normal force in each friction joint using the following local bang-bang controller

$$\begin{aligned} &F_{N_j} = F_{N_j}^{\min} + F_{N_j}^{\max}\, H\big[e_j\, u_{R_j}\big], \\ &F_{N_j}^{\min} \leqslant F_{N_j} \leqslant F_{N_j}^{\max} \end{aligned} \tag{34}$$

which updates the normal force F_{N_j} in the j-th friction force depending on the difference $e_j = u_{d_j} - u_{R_j}$ between the desired actuator force u_{d_j} and the actual friction force u_{R_j}. To avoid unwanted bang-bang behavior due to the Heavyside function $H(\cdot)$, a boundary layer can be introduced as has been done for the SISO controller defined by Eq. (32). In the following, the proposed controller is refered to as cLQG controller.

The approximation of the desired actuator forces is limited because of the dissipativity constraint and the boundedness of the friction force. If the measurement of the actual friction forces turns out to be difficult, the Kalman estimator can be extended by an integrator model [14] to estimate the friction forces, as well.

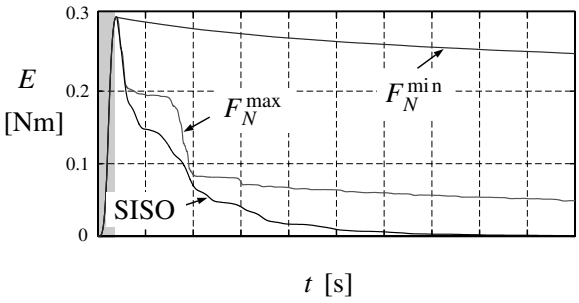

Fig. 12. System energy.

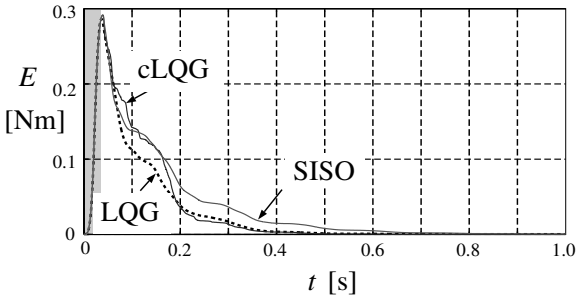

Fig. 13. System energy.

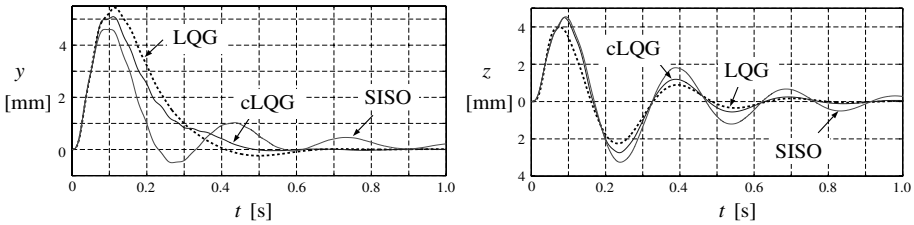

Fig. 14. Deflection of the mast tip: y-direction (left), z-direction (right).

6. Simulation results

The simulation results in this section will show the potential of the proposed semi-active approach to vibration suppression. The boundary conditions and disturbance (impulse force with an amplitude of $200\,\mathrm{N}$ over a time period of $40\,\mathrm{ms}$) are the same as described in the previous Section 4.3. Three semi-active friction joints are placed in order to affect the lower modes of the structure. The optimal locations for a specific mode are determined by considering the strain energies in the end connectors which occur when the structure is deformed according to the mode shape. Since the focus has been put on the lower modes, all semi-active joints are of type A. The replaced truss nodes and the corresponding members which are adaptively connected to them are marked in Fig. 11. It should be noted that if the vibration of the structure is dominated by modes not considered in the optimization of the joints' placement, their ability to enhance the damping of the vibration decreases accordingly.

The numerical model is reduced to 24 states using the proposed reduction method. The 24 states represent 9 modes and 3 additional 'correction modes' (Krylov vectors) generated for each friction joint.

Figure 12 compares the decay of the system energy E (defined by Eq. (34)) for the structure with passive and semi-active friction joints. A passive joint has a constant normal force which is set to either $F_N^{\min}$ or $F_N^{\max}$. For the semi-active joints the control law Eq. (32) with optimized control parameter ε_j is used. It should be noted that during the excitation time period, the normal forces are set to $F_N^{\max}$ in order to enable a comparison of the different

concepts. As can be seen, the damping can significantly be enhanced by controlling the normal forces in the friction joints. With a constant maximal normal force good vibration suppression is achieved at the beginning. However, as the vibration amplitude decreases sticking occurs and no energy is dissipated. Only the small structural damping reduces the vibrations.

The performance of the cLQG controller is shown in Fig. 13 together with the SISO controller. Furthermore, the response of a fully active system where the optimal actuator forces $\boldsymbol{u}_d$ are provided by the LQG controller (Eq. (35)) are directly applied to the structure. The corresponding tip deflections in y- and z-direction are given in Fig. 14.

When considering the system energy, the cLQG controller seems to perform only slightly better than the three SISO controllers. The advantage of the cLQG controller becomes more obvious when the tip deflections are compared (Fig. 14). In order to see how a fully active system would perform, the corresponding plots are included in Figures 13 and 14 as well. As can be seen, the suppression of the tip deflections provided by the LQG controller (active system) is only slightly better when compared to the cLQG controller (semi-active system), wheras the advantage of the cLQG controller over the three SISO controllers is significant. However, it is important to point out that the semi-active approach requires only a fraction of the control power of the active system.

7. Conclusions

The present semi-active approach to vibration suppression of large space truss structures is based on controlled energy dissipation in friction joints. A numerical model of the adaptive structure is presented, including the nonlinear dynamics of the friction joints. The finite element model of the truss structure is updated by using data from an Experimental Modal Analysis. And the parameters of the friction model are identified from measurements on an isolated friction joint. To obtain a low order model a reduction method is proposed which is a combination of balanced reduction and matching moments method. A numerical example illustrates the approximation quality of the reduced model. Two different control approaches for semi-active damping using friction joints are introduced. Finally, the simulation results of the truss structure with three semi-active friction joints demonstrate the efficiency of the present vibration suppression approach.

Acknowledgements

The authors gratefully acknowledge the funding of this research by the DFG (Deutsche Forschungsgemeinschaft) under grant GA209/24 “Adaptive control of mechanical joints in lightweight structures”.

References

[1] B. Armstrong-Hélouvry, P. Dupont and C.D. Wit, A survey of models, analysis tools and compensation methods for the control of machines with friction, *Automatica* **30**(7) (1994), 1083–1138.
[2] Z. Bai, Krylov subspace techniques for reduced-order modeling of large-scale dynamical systems, *Journal of Applied Numerical Mathematics* **43** (2002), 9–44.
[3] C. Canudas de Wit, H. Olsson, K.J. Ïström and P. Lischinsky, A new model for control of systems with friction, *IEEE Transactions on Automatic Control* **40**(3) (1995), 419–425.
[4] R.R. Craig Jr. and T.-J. Su, Model reduction and control of flexible structures using krylov vectors, *Journal of Guidance and Control* **14**(2) (1991), 260–267.
[5] S.J. Dyke et al., Lyapunov design of damping controllers, *Archive of Applied Mechanics* **5** (1996), 565–575.
[6] M.I. Friswell and J.E. Mottershead, *Finite Element Model Updating in Structural Dynamics*, Kluwer Academic Publishers, Dordrecht, 1995.
[7] L. Gaul, H. Albrecht and J. Wirnitzer, Damping of structural vibrations using adaptive joint connections and neural control, in: *CISM Courses and Lectures: Smart Structures*, A. Suleman, ed., No. 429, 2001, pp. 86–97, Udine, Italy.
[8] L. Gaul and R. Nitsche, Friction control for vibration suppression, *Mechanical Systems and Signal Processing* **14**(2) (2000), 139–150.
[9] L. Gaul and R. Nitsche, The role of friction in mechanical joints, *Applied Mechanics Reviews* (*ASME*) **54**(2) (2001), 93–106.
[10] L. Gaul and R. Nitsche, Lyapunov design of damping controllers, *Archive of Applied Mechanics* **72** (2003), 865–874.
[11] W.K. Gawronski and J.-N. Juang, Model reduction for flexible structures, *Control and Dynamic Systems: Advances in Theory and Application* **36** (1990), 143–222.

[12] C.Z. Gregory Jr., Reduction of large flexible spacecraft models using internal balancing theory, *Journal of Guidance and Control* **7**(6) (1984), 725–732.
[13] M. Hanss, S. Oexl and L. Gaul, Simulation and analysis of structural joint models with uncertainties, in: *Proc. of the International Conference on Structural Dynamics Modeling – Test, Analysis, Correlation and Validation*, (Madeira Island, Portugal), 2002, pp. 165–174.
[14] R. Hu and P.C. Müller, Position control of robots by nonlinearity estimation and compensation: Theory and experiements, *Journal of Intelligent and Robotic Systems* **20** (1997), 195–209.
[15] R.E. Kalman and R. Bucy, New results in linear filtering and prediction, *ASME Journal of Basic Engineering* **83** (1961), 95–108.
[16] A.R. Kukreti and H.I. Issa, Dynamic analysis of nonlinear structures by pseudo-normal mode superposition method, *Computers & Structures* **19**(4) (1984), 643–663.
[17] H. Kwakernaak and R. Sivan, *Linear Optimal Control Systems*, Wiley, New York, 1972.
[18] J.S. Lane, A.A. Ferri and B.S. Heck, Vibration control using semi-active friction damping, in *Friction-induced vibration, chatter, squeal, and chaos*, *ASME* **49** (1992), 165–171.
[19] B.C. Moore, Principal component analysis in linear systems: Controllability, observability, and model reduction, *IEEE Transactions on Automatic Control* **AC-26**(1) (1981), 17–32.
[20] J. Onoda, T. Sano and K. Minesugi, Passive damping of truss vibration using preloaded joint backlash, *AIAA Journal* **33**(7) (1995), 1335–1341.
[21] J. Wirnitzer, A. Kistner and L. Gaul, Optimal placement of semi-active joints in large space truss structures, in: *SPIE Conference on Smart Structures and Materials 2002: Damping and Isolation*, G.S. Agnes, ed., No. 4697, (San Diego, USA), 2002, pp. 246–257.